Surface Properties and Catalytic Performance of Pt/PrSrCoO$_4$ Catalysts for NO Reduction by CO

Hua ZHONG[*], **Xirui ZENG**

Department of Chemistry, Jinggangshan College, Jian, 343009, PR CHINA
e-mail: hua_zh@163.com

Perovskite-type $Pr_{2-x}Sr_xCoO_{4\pm\lambda}$ mixed oxides were prepared by different calcination temperatures and were investigated by XRD, BET, TPD, TPR and XPS methods. These catalysts possess high catalytic activities towards the NO reduction by CO, and the activity of the PrSrCoO$_4$ catalyst prepared by calcining at 750 °C is the best among these samples. This is explained in terms of its greater oxygen vacancies and larger BET surface areas. The influence of modification by a suitable amount of Pt-doping on the surface properties and catalytic activity for NO reduction by CO was studied. The results show that the Pt-modified PrSrCoO$_4$ catalysts display activity significantly higher than that of the Pt-free system PrSrCoO$_4$. Characterization of the catalysts by XRD, TPD, TPR and XPS methods reveals that both the surface and the bulk phase of the perovskite-type PrSrCoO$_4$ play important roles in the catalytic activities for NO reduction by CO.

Key Words: Perovskite-type A$_2$BO$_4$, Pt/PrSrCoO$_4$, XPS, NO reduction by CO.

Introduction

Perovskite oxides, ABO$_3$, have been extensively investigated. Among the reactions of particular interest is the reduction of NO by CO since both gases usually exist in effluent gas mixtures. As a result, the de-NO$_x$ reaction in the presence of CO has been studied by a number of researchers on various perovskite oxides[1−4]. However, the perovskite-type A$_2$BO$_4$ mixed oxides of K$_2$NiF$_4$ structure consisting of alternating layers of ABO$_3$ perovskite and AO rock salt show high catalytic activity in the reactions involved in motor vehicles' exhaust gas after treatment, and are recently studied as new materials for their low cost, high catalytic activity and high thermal stability[5]. Many studies have shown that the catalytic performances of A$_2$BO$_4$ mixed oxides, to a large extent, are associated with the species of A-site and B-site ions, and their corresponding valences, and the crystal structure of these oxides as well[6]. It is noted that there are many reports in the literature contributing to investigations of A$_2$BO$_4$ catalysts[7,8]. Actually, the studies involving the investigation of A$_2$BO$_4$ mixed oxides are extremely limited. Moreover, almost no literature has been dedicated to noble metals supported on monoliths or perovskite-type used as 3-way catalysts for

---

[*]Corresponding author

NO reduction by CO, although the perovskite-type system in pure form is promising. Therefore, further investigation is necessary.

We have already studied the catalytic oxidations of CO and C_3H_8 over perovskite-type $LnSrCoO_4$(Ln = La, Pr, Nd, Sm, Eu) mixed oxides[9−12]. The work presented in this study is a continuation of the studies performed in our laboratory on $LnSrCoO_4$. In this paper, using the citric acid sol-gel method and impregnating method, a series of catalysts were prepared and characterized. With NO reduction by CO as testing reactions, the catalytic performances of all these catalysts were investigated. To show the probable intrinsic performances, XRD, BET, TPD, TPR and XPS were employed.

Experimental

Preparation of catalysts

The perovskite-type $Pr_{2-x}Sr_xCoO_{4\pm\lambda}$ catalysts were prepared by the citric acid sol-gel method. Briefly, praseodymium, strontium, and cobalt nitrates in a Pr:Sr:Co nominal molar ratio of 2-x:x:1.0 (x = 0.2, 0.4, 0.6, 0.8, 1.0) were dissolved in a citric acid solution at 80 °C with constant stirring. The polyglycol 20,000 was added in when the solution was evaporated to 40 mL. The stirring was continued until a viscous gel was formed. The resulting gel was evaporated to dryness, and the obtained precursor was calcined at 550 °C for 4 h, followed by pelletization and calcination once more at 950 °C (or 750, 850 °C) in air for 10 h.

γ-Al_2O_3-supported (γ-Al_2O_3 was crushed and sieved to 0.250 ± 0.800 mm and calcined overnight at 500 °C) Pt and x% (wt%) $PrSrCoO_4$ catalysts, marked as Pt/γ-Al_2O_3 and x% $PrSrCoO_4$/γ-Al_2O_3, were prepared by impregnating a γ-Al_2O_3 carrier (surface area, 108.9 m^2/g) with an aqueous solution containing the desired molar ratio of praseodymium, strontium, cobalt nitrates, and citric acid, followed by drying at 110 °C for 4 h and then calcining at 750 °C in air for 6 h.

Pt-modified $PrSrCoO_4$ catalysts, marked as y% Pt/$PrSrCoO_4$, were prepared by wet impregnating with y% (wt%) Pt, followed by drying at 110 °C for 4 h and then calcining at 550 °C in air for 6 h. All samples were pulverized to ca. 60-80 mesh size.

Characterization of catalysts

A powder X-ray diffractometer (D8/ADVANCE, Germany) over the range $20° \geq 2\theta \geq 80°$, at ambient temperature, was operated at 40 kV/10 mA, using Cu K_α radiation combined with a nickel filter.

The XPS analysis was carried out on a PHI 5000C ESCA X-ray photoelectron spectrometer using Al K_α radiation under a vacuum of 1.3×10^{-7} Pa at 14 kV/20 mA. The effect of surface charge on the binding energy was corrected by using polluted carbon peak C_{1s}= 285.00 eV.

Specific areas were calculated by the BET method from the nitrogen adsorption isotherms, recorded at liquid nitrogen temperature on the equipment ST-2000 (China), taking a value of 0.16 nm^2 for the cross-sectional area of the N_2 molecule adsorbed at -196 °C.

Temperature programmed desorption (TPD) experiments were carried out in an automatic Micromeritics 3000 equipment interfaced to a data station. Under O_2 gas, catalyst samples (300 mg) were heated from ambient temperature to 950 °C at a rate of 8 °C/min and subsequently left for 1 h. When the system had cooled down to ambient temperature, He gas (carrier gas) was used to remove the O_2 in the

gas phase. Subsequently, with the rate of 8 °C/min, the curves of O_2-absorbed desorption were recorded by on-line chromatography.

Temperature programmed reduction (TPR) experiments were carried out in the same apparatus with TPD. The samples (100 mg) were first heated to 950 °C at a rate of 20 °C/min in a flow of N_2 (99.9%) gas and then cooled to ambient temperature. After being 10% H_2/N_2-purged for 1 h, at the rate of 20 °C/min, the curves of H_2 reduction were recorded by on-line chromatography.

Activity measurement of catalysts

The catalytic activities (catalyst load 250 mg, particle size 60-80 mesh) were determined at atmospheric pressure in an automatic Micromeritics flow reactor with a reaction mixture containing NO (2.02% vol-%), CO (1.99% vol-%), He (balance), and total GHSV (8000 h^{-1}). The gas composition was analyzed before and after the reaction by on-line gas chromatography with a thermal conductor detector (TCD) and connected to a computer integrator system using a TDX-01 (2 m) column for N_2, CO and NO, and a Porapak Q (3 m) column for CO_2 and N_2O. The ambient temperatures for columns and TCD are 50 °C and 75 °C, respectively. The formation of N_2O was hardly detected for all of the catalysts tested in this work. The catalytic activity and selectivity to N_2 were calculated by the following respective equations:

Conversion of NO = ($[NO]_{in}$ - $[NO]_{out}$) / $[NO]_{in}$ × 100%

Selectivity of N_2 = $2[N_2]$ / ($[NO]_{in}$ - $[NO]_{out}$) × 100%.

Results and Discussion

Optimization of $Pr_{2-x}Sr_xCoO_{4\pm\lambda}$ catalysts' composition and preparation conditions

The XRD patterns of $Pr_{2-x}Sr_xCoO_{4\pm\lambda}$ catalysts are displayed in Figure 1. These patterns correspond mainly to perovskite-type structures. However, for $Pr_{2-x}Sr_xCoO_{4\pm\lambda}$ catalysts (x = 0.2 and 1.0), diffraction peaks other than the perovskite-type ones are observed. These new peaks of low intensity are indexed to CoO, Pr_2O_3 or $SrCO_3$ phases. As is well known, A_2BO_4 mixed oxides of K_2NiF_4 structure can be classified specially into 2 forms, i.e. F/mmm orthorhombic-phase and I4/mmm tetragonal-phase, and the I4/mmm tetragonal-phase can be classified further into 3 phases (T, T*, T')[13]. An analogous result can also be obtained from the XRD patterns of $Pr_{2-x}Sr_xCoO_{4\pm\lambda}$ catalysts. As shown in Figure 1, for the $Pr_{2-x}Sr_xCoO_{4\pm\lambda}$ catalysts with x = 0.2 and 0.4, only the diffraction peaks attributed to the T phase of I4/mmm tetragonal-phase are observed, while with x increased to 1.0, weak peaks attributed to the discrete T* phase of I4/mmm tetragonal-phase are also detected. As the same time, the peaks due to the K_2NiF_4 structure phase get stronger and sharper as the calcination temperature increases, indicating an increase in the degree of long-range order in the perovskite-type lattice and the growing of crystallites. However, the lower the calcination temperature is, the more the T* phase appears. Moreover, we still find that the T* phase results from abundant oxygen vacancies, and more oxygen vacancy is favorable for catalytic activity. Therefore, as shown in Table 1, a suitable proportion of substitution of Sr^{2+} for Pr^{3+} results in improvements in NO conversion and selectivity to N_2, with the activity of the $PrSrCoO_4$ catalyst prepared by calcining at 750 °C (with a relatively large surface area of 10.16 m^2/g and much nonstoichiometric oxygen (λ)–0.27) being the highest.

Table 1. Catalyst characteristics and catalytic behavior for NO reduction by CO.

X in catalyst	Calcination temperature (°C)	Structure	BET surface area (m²/g⁻¹)	Nonstoichiometric (°C)	T_{50} (°C)	T_{99} (°C)	S_{N2}(%) (°C)
0.2	950	T,Pr$_2$O$_3$,CoO	2.34	+0.12	315	450	55
0.4	950	T	2.41	+0.03	300	405	59
0.6	950	T, T*	2.49	-0.04	290	400	64
0.8	950	T, T*	2.53	-0.09	280	390	68
1.0	950	T,T*, SrCO$_3$	2.84	-0.18	270	375	73
1.0	850	T,T*, SrCO$_3$	5.93	-0.22	265	360	77
1.0	750	T,T*, SrCO$_3$	10.16	-0.27	255	340	82
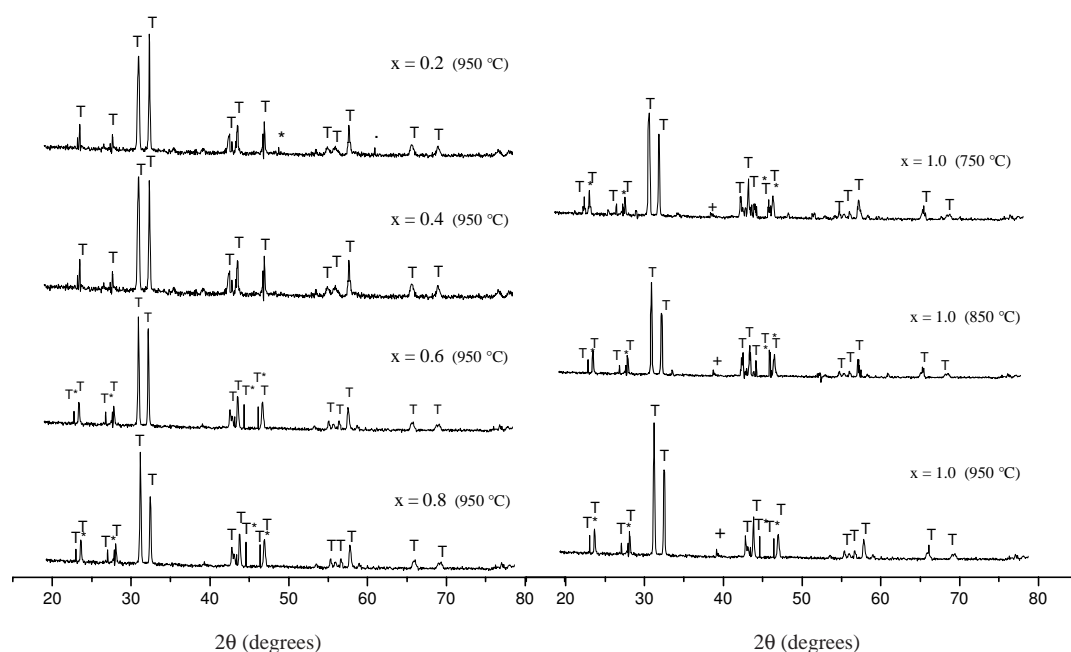
Figure 1. XRD patterns of the Pr$_{2-x}$Sr$_x$CoO$_{4\pm\lambda}$ catalysts T: T phase, T*: T* phase, +:SrCO$_3$,*:Pr$_2$O$_3$,˙: CoO.

The O$_2$ TPD profiles for Pr$_{2-x}$Sr$_x$CoO$_{4\pm\lambda}$ catalysts are shown in Figure 2. In all these profiles can be observed a broad and strong O$_2$ desorption over 600 °C (β peak), and the intensity of the O$_2$-desorption peak increases from sample x= 0.2 to sample x= 1.0. For substitution degree x= 0.6-1.0, the O$_2$-desorption peak, which shifts to ca. 350 °C ($\alpha^{'}$ peak), is accompanied by a shoulder around 200 °C (α peak). Generally, the α peak exists possibly due to the ordinarily chemically adsorbed oxygen (O$_2$, O$_2^-$) on the surface of the catalyst, and the $\alpha^{'}$ peak can be related to the chemically adsorbed oxygen (O$^-$) in the oxygen vacancies of the catalyst. The release of oxygen vacancies can be due to the reduction of Co^{3+}:

$$2Co^{3+} + O^{2-} \rightarrow 2Co^{2+} + 1/2O_2 + V_o.$$
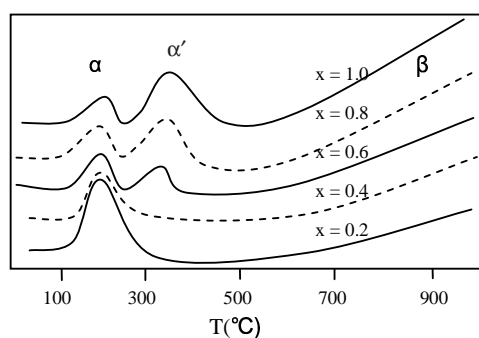
Figure 2. TPD patterns of the $Pr_{2-x}Sr_xCoO_{4\pm\lambda}$ catalysts.

The β peak corresponds to the release of oxygen (O^{2-}) in the lattice of the catalyst[14]. This coincides with the results obtained from the XRD study.

The TPR profiles of $Pr_{2-x}Sr_xCoO_{4\pm\lambda}$ catalysts are displayed in Figure 3. All the samples show similar reduction profiles consisting of 3 sets of peaks (α, β and γ), respectively. Since both Pr^{3+} and Sr^{2+} are nonreducible under the conditions of the experimental section, the observed H_2-TPR peaks should be due to the reduction of Co^{n+} species. The trivalent ion Pr^{3+} at the A site is substituted by a lower valent ion Sr^{2+}, according to the principle of electroneutrality[15]. The positive charge reduced could be balanced either by the formation of higher oxidation state at the B site, i.e. Co^{2+} to Co^{3+}, or by the formation of oxygen vacancy (Vo). The peak α corresponds to reduction of the nonstoichiometric oxygen (λ) and also to some oxygen from the perovskite-type structure. With the increase in x, the nonstoichiometric oxygens obtained from the total hydrogen consumption are 0.14, 0.07, -0.01, -0.08 and -0.16, respectively. These results are similar to those obtained by chemical analyses (Table 1). The peak β could be attributed to reduction of Co^{3+} into Co^{2+}, and the partially reduced $Pr_{2-x}Sr_xCoO_{4\pm\lambda}$ intermediate produced still preserves the perovskite-type phase structure as a whole[16]. The peak γ might be attributed to the reduction of Co^{2+}, i.e. Co^{2+} to Co^0, which leads to the breakdown of the perovskite-type phase and formation of the discrete phases, Pr_2O_3, SrO, and Co. This interpretation is also supported by the XRD patterns, which show the appearance of small amounts of crystalline Co phase.
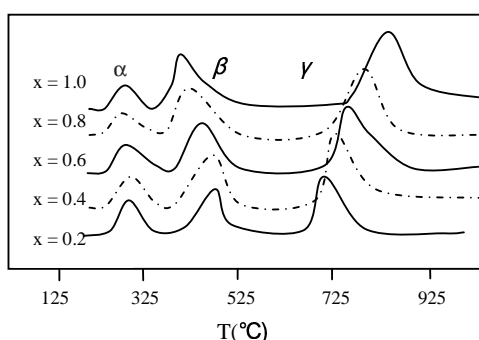
Figure 3. TPR patterns of the $Pr_{2-x}Sr_xCoO_{4\pm\lambda}$ catalysts.

Table 2 lists the corresponding binding energies for $Pr_{3d5/2}$, $Co_{2p3/2}$, $Sr_{3d5/2}$ and O_{1s} of the $Pr_{2-x}Sr_x$ $CoO_{4\pm\lambda}$ (x = 0.6-1.0) and the $PrSrCoO_4$ catalysts prepared by calcinations at different temperatures. In addition, the molar percentage of cations of the 3 kinds of component elements on the surface is estimated and listed in Table 2 according to Wagner et al.[17] for the Mg K_a source. From Table 2, it is known that

the binding energy for $Pr_{3d5/2}$ is constant for all samples, which indicates that calcination temperature or substitution of Sr^{2+} in the perovskite-type structure does not appear to affect to a significant extent the binding energy of $Pr_{3d5/2}$ level. The binding energy of $Co_{2p3/2}$ displays 2 species. The binding energies of these component elements are in good agreement with those reported in the literature[18-20]. The results obtained from the XPS investigation show that the measured binding energy for $Co_{2p3/2}$ deviates gradually from the value of Co^{2+} with the increase in x or with the decrease in calcination temperature, which indicates that the surface concentration of Co^{2+} decreases gradually and the surface concentration of Co^{3+} increases gradually at the same time. On the other hand, the Co/(Pr+Sr) surface ratios for the samples are much higher than expected, considering the nominal compositions, and they increase gradually with the increase in x or with the decrease in calcination temperature. These results suggest that enrichment of the Co cation on the surface occurs for all samples, and that the surface concentration of Co increases with the increase in x or with the decrease in calcination temperature. The O_{1s} spectra for all 5 samples include 2 signals, with the binding energy approaching 529.0 and 531.1 eV, respectively, and the binding energy approaching 531.1 eV increases with the increase in x or with the decrease in calcination temperature. The former may be ascribed to the lattice oxygen species, while the latter may originate from the chemisorption oxygen, i.e. the oxygen chemically adsorbed on oxygen vacancies[21]. The XPS analysis coincides with the results obtained from the O_2-TPD study.

Table 2. XPS Pr_{3d}, Sr_{3d}, Co_{2p} and O_{1s} binding energies and surface compositions of catalysts.

Catalyst	XPS-BE (eV)*				Surface cation molar percentage			Co/(Pr+Sr)
	$Pr_{3d5/2}$	$Sr_{3d5/2}$	$Co_{2p3/2}$	O_{1s}	Pr	Sr	Co	(mol/mol)
$Pr_{1.4}Sr_{0.6}CoO_{3.96}$ (950 °C)	933.6	134.1	780.3	529.0 530.8	26.2	30.3	43.5	0.77
$Pr_{1.2}Sr_{0.8}CoO_{3.91}$ (950 °C)	934.0	134.3	779.8	529.1 531.2	20.1	33.6	46.3	0.86
$PrSrCoO_{3.82}$ (950 °C)	933.9	133.9	779.5	528.8 531.3	14.3	36.1	49.6	0.98
$PrSrCoO_{3.78}$ (850 °C)	934.1	133.6	779.2	528.9 531.4	12.6	37.0	50.4	1.02
$PrSrCoO_{3.73}$ (750 °C)	933.7	133.8	778.9	528.7 531.6	9.5	37.3	53.2	1.14

*Calibrated internally by the carbon deposit C_{1s} at 285.00 eV (BE).

The above results indicate that the catalytic activity for NO reduction by CO is closely related to the surface area, and the phase and oxygen vacancy of the catalyst, as well as the concentration of Co on the surface of the catalyst. The perovskite-type $PrSrCoO_4$ catalyst prepared by calcination at 750 °C displays relatively good catalytic activity for NO reduction by CO, and is thus selected as the host catalyst for modification by platinum in the following work.

Catalytic activities for NO reduction by CO of the Pt-modified $PrSrCoO_4$-based catalysts

The results of NO reduction by CO over $Pt/PrSrCoO_4$ catalysts and related systems are summarized in Table 3 by means of the 50% and 99% conversion temperatures of NO (T_{50}, T_{99}) and the selectivity to N_2.

By comparing the evaluation of the Pt-doping and Pt-undoping systems, it is evident that the modification of platinum to the $PrSrCoO_4$ catalyst improved the performance of the catalyst for NO reduction by CO. The T_{50} and T_{99} temperatures of the 3% $Pt/PrSrCoO_4$ catalyst for NO reduction by CO decrease to 225 and 258 °C from 255 and 340 °C, respectively, for Pt-free systems. Even at such a low reaction temperature, the selectivity to N_2 is close to 95%. In addition, the evaluation results of the catalysts with different Pt-doping amounts show that the NO conversion activity and the selectivity to N_2 increase initially with increasing Pt-doping amount, and approach a stable level with 3% of Pt-doping. It seems that 3% of Pt-doping is appropriate for the $PrSrCoO_4$ catalyst prepared by calcination at 750 °C. On the other hand, the conversion activity of NO and the selectivity to N_2 over all these γ-Al_2O_3-supported $PrSrCoO_4$ systems are lower than that of the unsupported 100% $PrSrCoO_4$ system. Moreover, the conversion activity of NO and the selectivity to N_2 increase, although the surface area of supported catalysts decrease greatly with the increasing $PrSrCoO_4$-loading ratio. This implies that not only the surface but also the bulk perovskite-type phase plays an important role in the catalytic activities of NO reduction by CO.

Table 3. Catalytic behavior for NO reduction by CO over $Pt/PrSrCoO_4$ catalysts and related systems.

Catalyst	T_{50} (°C)	T_{99} (°C)	S_{N2}(%) (320 °C)
10% $PrSrCoO_4/\gamma$-Al_2O_3	325	483	48
20% $PrSrCoO_4/\gamma$-Al_2O_3	299	432	64
25% $PrSrCoO_4/\gamma$-Al_2O_3	278	398	70
33% $PrSrCoO_4/\gamma$-Al_2O_3	264	365	75
100% $PrSrCoO_4$	255	340	82
0.1% $Pt/PrSrCoO_4$	250	330	85
1% $Pt/PrSrCoO_4$	246	312	87
2% $Pt/PrSrCoO_4$	240	290	91
3% $Pt/PrSrCoO_4$	225	258	95
5% $Pt/PrSrCoO_4$	237	289	89
3% Pt/γ-Al_2O_3	223	270	85

The elementary steps of the reaction NO + CO, irrespective of its taking place on perovskites or supported noble metals, are generally accepted to proceed according to the following sequence of elementary reactions[22].

$$NO_g \rightarrow NO_{ads} \tag{1}$$

$$NO_{ads} \rightarrow N_{ads} + O_{ads} \tag{2}$$

$$CO_g \rightarrow CO_{ads} \tag{3}$$

$$CO_{ads} + O_{ads} \rightarrow CO_2 \tag{4}$$

$$2N_{ads} \rightarrow N_2 \tag{5}$$

$$N_{ads} + NO_{ads} \rightarrow N_2O_{ads} \tag{6}$$

$$N_2O_{ads} \rightarrow N_2 + O_{ads} \tag{7}$$

The most important single parameter, which seems to influence the catalytic activities, is the excess or deficiency of oxygen in the perovskite-type structure. The oxygen vacancies are beneficial to the regeneration of active site for NO reduction by CO.

Characterization of the Pt-modified PrSrCoO$_4$-based catalysts

Figure 4b, c and d show the XRD patterns of the 3 Pt-modified PrSrCoO$_4$ catalysts. By contrast with the PrSrCoO$_4$ catalyst (see Figure 4a), besides the features ascribed to the perovskite-type structure, 2 weak peaks at $2\theta = 26.05$ and 42.70 are observed, which become more pronounced as the Pt-doping percentage increases from 1% to 3%. This is in agreement with the known 2θ values for PtCl$_4$, and thus can be attributed to the crystallite phase of PtCl$_4$. In addition, for 3% Pt/PrSrCoO$_4$ and 5% Pt/PrSrCoO$_4$ catalysts, peaks at 39.80, 46.30 and 67.55, which are ascribed to the XRD characteristic peak of the Pt phase, are identified in Figure 4c and d. However, there is no conclusive evidence for the existence of a Pt crystallite phase on the catalyst of 1% Pt-modified PrSrCoO$_4$.
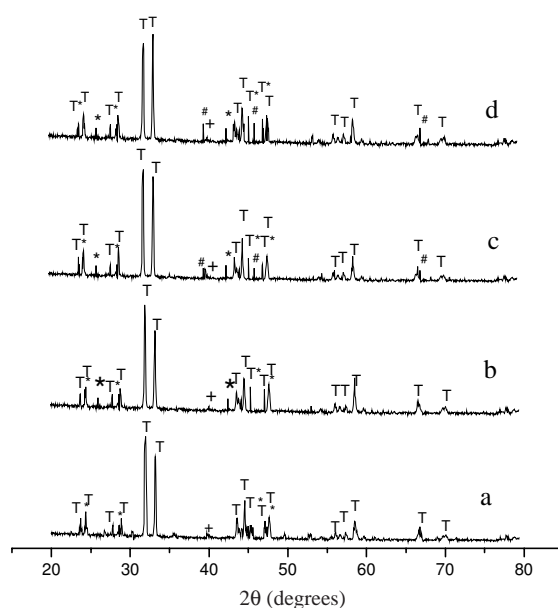
Figure 4. XRD patterns of the catalysts T: T phase, T*: T* phase, +:SrCO$_3$, *:PtCl$_4$, #: Pt. a: PrSrCoO$_4$; b: 1% Pt/PrSrCoO$_4$; c: 3% Pt/PrSrCoO$_4$; d: 5% Pt/PrSrCoO$_4$.

The results of the O$_2$-TPD investigation (in Figure 5) show that an obvious difference existed between the 2 catalysts doping and undoping by Pt in their adsorption/desorption behavior to oxygen. For the 3% Pt/PrSrCoO$_4$ catalyst, 2 much stronger peaks at 80 and 220 °C are observed besides the 200, 375 and over 600 °C peaks, compared to that of the Pt-free system PrSrCoO$_4$, while the 200, 375 and over 600 °C peaks for the Pt-doping systems are very close to that for the Pt-free system in position and intensity. They probably originate from desorption of the same kind of strongly adsorbed oxygen species. The strong peaks at 80 and 220 °C for the Pt-doping system are evidently related to the doping of H$_2$PtCl$_6$ in PrSrCoO$_4$. Therefore, the O$_2$-TPD results clearly indicate that the doping of H$_2$PtCl$_6$ in the PrSrCoO$_4$ catalyst would lead to enhancement of adsorbability of the catalyst towards oxygen, and result in generating plenty of oxygen ad-species that can be desorbed, meaning that the quantity of adsorbed and nonstoichiometric oxygen species being able to participate in the NO reduction by CO would greatly increase.
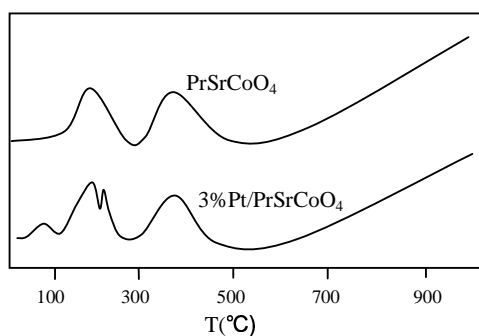
Figure 5. TPD patterns of the $PrSrCoO_4$ and 3% $Pt/PrSrCoO_4$ catalysts.

The TPR profiles of the $PrSrCoO_4$ and 3% $Pt/PrSrCoO_4$ catalysts are displayed in Figure 6. Comparing with that of the Pt-free system $PrSrCoO_4$, the reduction profile of the 3% $Pt/PrSrCoO_4$ catalyst is more one peak at 130 °C, which could be attributed to reduction of PtO_2^{23}. At the same time, the high temperature (810 °C) reduction peak of the 3% $Pt/PrSrCoO_4$ catalyst, which leads to the breakdown of the perovskite-type phase, is unchanged in position and shape, compared with that of the $PrSrCoO_4$. However, the downshift of the low temperature (290 and 400 °C) reduction peaks and the increment of their peak area are both apparent. Through the above comparison, we think that the doping of Pt greatly improved the low-temperature reducibility of the perovskite-type $PrSrCoO_4$, remarkably increasing the content of low-temperature-reducible Co^{3+} species.
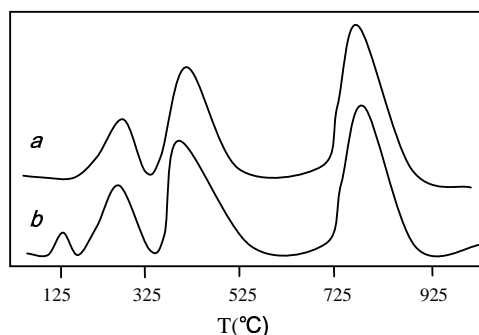
Figure 6. TPR patterns of the $PrSrCoO_4$ and 3% $Pt/PrSrCoO_4$ catalysts a: $PrSrCoO_4$; b: 3% $Pt/PrSrCoO_4$.

Figure 7 shows the XPS spectra of Co_{2p} of the $PrSrCoO_4$ and 3% $Pt/PrSrCoO_4$ catalysts. There are 2 peaks at 780.8 and 795.5 eV for the both samples, respectively. The former was evidently due to Co^{2+} (2p). The latter could be ascribed to Co^{3+} (2p)[20]. The peak area at 795.5 eV for 3% $Pt/PrSrCoO_4$ catalyst is higher than that of $PrSrCoO_4$ catalyst, which indicates that the surface concentration of Co^{3+} increases after the doping of H_2PtCl_6 in the $PrSrCoO_4$. In addition, for the sake of clarity the influence of doping Pt onto $PrSrCoO_4$, the O_{1s} curves of $PrSrCoO_4$ and 3% $Pt/PrSrCoO_4$ are shown in Figure 8. The O_{1s} curves of the 2 catalysts include 2 peaks at 529.0 and 531.1 eV, respectively, and the peak areas of 3% $Pt/PrSrCoO_4$ approaching the binding energy (531.1 eV) are higher than that of $PrSrCoO_4$. Since the peak of O_{1s} curves approaching the binding energy (531.1 eV) may originate from the oxygen chemically adsorbed on oxygen vacancies, the oxygen vacancies of 3% $Pt/PrSrCoO_4$ are more than those of $PrSrCoO_4$. On the other hand, for the sake of even more clarity the influence of doping Pt onto $PrSrCoO_4$, the Pt (4f)-XPS spectra of the

Pt/PrSrCoO$_4$ catalysts are shown in Figure 9, in which 2 peaks at 75.5 and 71.2 eV are observed. The peak at 71.2 eV is somewhat strengthened with the increase in Pt-doping percentage from 3% to 5%. According to the literature[24], and the above XRD characterization of the Pt/PrSrCoO$_4$ catalysts, the peak observed at 71.2 eV is assigned to Pt (4f) of metallic platinum species. From the fact that the binding energy of the main peak observed at 75.5 eV was consistent with that assigned to Pt (4f) of PtCl$_4$ in the literature[24], we suggest that most of the Pt species on the surface layer of the Pt-doping PrSrCoO$_4$ system is Pt^{4+}. These results indicate that the catalytic activity for NO reduction by CO is closely related to the oxygen vacancy of the catalyst, as well as the concentration of Co^{3+} on the surface of the catalyst.
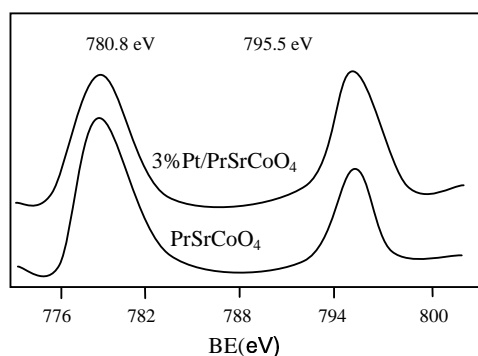
Figure 7. XPS patterns of Co$_{2p}$ of the PrSrCoO$_4$ and 3% Pt/PrSrCoO$_4$ catalysts.
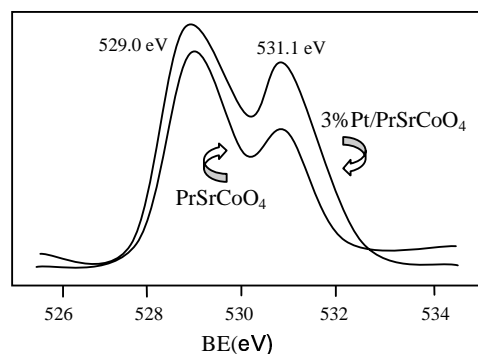
Figure 8. XPS patterns of O1s of the PrSrCoO$_4$ and 3% Pt/PrSrCoO$_4$ catalysts.
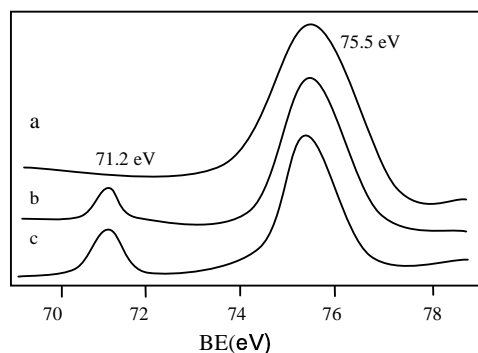
Figure 9. XPS patterns of Pt$_{4f}$ of the Pt/PrSrCoO$_4$ catalysts a: 1% Pt/PrSrCoO$_4$; b:3% Pt/PrSrCoO$_4$; c:5% Pt/PrSrCoO$_4$.

Acknowledgments

References

1. R.J.H. Voorhoeve, J.P. Remeika, L.E. Trimble and P.K. Gallagher, **J. Sol. State. Chem., 14,** 395-402 (1975).

2. D. Ferri, L. Forni, M.A.P. Dekkers and B.E. Nieuwenhuys, **Appl. Catal. B, 16,** 339-345 (1998).

3. Y. Yokoi and H. Uchida, **Catal. Today, 42,** 167-174 (1998).

4. J.M.D. Tascon, L.G. Tejuca and C.H. Rochester, **J. Catal., 95,** 558-564 (1985).

5. S.D. Peter, E. Garbowski, N. Guilhaume, V. Perrichon and M. Primet, **Catal. Lett., 54,** 79-84 (1998).

6. Y. Liu, X.G. Yang, Y.M. Liu and Y. Wu, **Acta. Phy-chim. Sin., 15,** 506-511 (1999).

7. Y. Wu, Z. Zhao, Y. Liu and X. Yang, **J. Mol. Catal. A: Chemical, 155,** 89-100 (2000).

8. Z. Zhao, X.G. Yang, Y. Liu and Y. Wu, **J. Chin. Rare Earth. Soc., 16**, 325-331 (1998).

9. X.M. Yang, L.T. Luo and H. Zhong, **Appl. Catal. A: General, 272,** 299-303 (2004).

10. L.T. Luo, H. Zhong and X.M. Yang. **J. Serb. Chem. Soc., 69,** 783-790 (2004).

11. X.M. Yang, L.T. Luo and H. Zhong, **React. Kinet. Catal. Lett., 81,** 219-227 (2004).

12. X.M. Yang, L.T. Luo and H. Zhong, **Catal. Communications, 6,** 13-17 (2005).

13. Y. Tokura, H. Takagi and S. Uchida, **Nature, 337,** 345-351 (1989).

14. Z. Zhao, X. Yang and Y. Wu, **Appl. Catal. B, 8,** 281-297 (1996).

15. Y. Wu, T. Yu, B.S. Dou and C.X. Wang, **J. Catal., 120,** 88-93 (1989).

16. R.J.H. Voorhoeve, **"Advanced Materials in Catalysis"**, p. 132. Academic Press, New York, London. 1977.

17. C.D. Wagner, L.E. Davis, M.V. Zeller, J.A. Taylor, R.H. Raymond and L.H. Gale, **Surf. Interface Anal. 3,** 211-216 (1981).

18. X.H. Yan, G.H. Rao and J.K. Liang, **Chin. Sci, Bull., 39,** 896-901 (1994).

19. K. Tabata and I. Matsumoto, **J. Mater. Sci., 22,** 1882-1887 (1987).

20. Y. Olamoto and T.Imanaka, **Appl. Catal. B, 73,** 249-254 (1991).

21. H. Taguchi, A. Sugita and M. Nagao, **J. Sol. State. Chem., 119,** 164-168 (1995).

22. A.K. Ladavos and P.J. Pomonis, **Appl. Catal. A: General, 165,** 73-85 (1997).

23. T. Huizinga, J. Grondelle and R. Prins, **Appl, Catal. B, 10,** 199-205 (1984).

24. Y.T. Yu and B.Q. Xu, **Acta. Chem. Sin., 61,** 1758-1764 (2003).